Nucleic Acids Research, 2026, **54**, gkag633
https://doi.org/10.1093/nar/gkag633
Chemical Biology and Nucleic Acid Chemistry

A turn-on fluorescent nucleoside enabling sequence-insensitive DNA labeling

Jinsi Li[1,2,†], Ziwen Dai[1,†], Lei He[1], Jiaxin Xu[3], Chenghe Xiong[1], Junlin Wen[1], Jingwei Zhou[4], Xuan Feng[1], Xue Chen[1], Xia Li[1], Lu Zhou[1], Chenguang Lou[5], Xiaoluo Huang[1,6,*], Xin Ming[2,*], Hui Mei[1,*]

[1]Shenzhen Key Laboratory of Synthetic Genomics, Guangdong Provincial Key Laboratory of Synthetic Genomics, State Key Laboratory of Quantitative Synthetic Biology, Shenzhen Institute of Synthetic Biology, Shenzhen Institutes of Advanced Technology, Chinese Academy of Sciences, Shenzhen 518055, China
[2]Key Laboratory of Structure-Specific Small Molecule Drugs at Chengdu Medical College of Sichuan Province, School of Pharmacy, Chengdu Medical College, Chengdu 610500, China
[3]Department of Pulmonary and Critical Care Medicine, Institute of Respiratory Diseases, Post-Doctoral Scientific Research Station of Basic Medicine, Shenzhen People's Hospital (The Second Clinical Medical College, Jinan University, The First Affiliated Hospital of Southern University of Science and Technology), Shenzhen, Guangdong 518020, China
[4]Department of Quantum Chemistry, Wecomput Technology Company, Ltd. (Guangzhou), Guangzhou 100085, P.R. China
[5]Biomolecular Nanoscale Engineering Center, Department of Physics, Chemistry and Pharmacy, University of Southern Denmark, Campusvej 55, Odense M 5230, Denmark
[6]Hubei Hongshan Laboratory; Institute of Computational Synthetic Biology, College of Informatics, Huazhong Agricultural University, Wuhan 430070, China

*To whom correspondence should be addressed. Email: hui.mei@siat.ac.cn
Correspondence may also be addressed to Xin Ming. Email: mingxin@cmc.edu.cn
Correspondence may also be addressed to Xiaoluo Huang. Email: huangxl@siat.ac.cn
†Jinsi Li and Ziwen Dai contributed equally to this work.

Abstract

Fluorescent nucleobase analogs (FBAs) are valuable tools for studying nucleic acid structure and dynamics. However, their utility is often limited by substantial fluorescence quenching upon incorporation into oligonucleotides and variable brightness influenced by neighboring bases. In this study, we present a novel turn-on nucleoside, 3b, a thiazolyl-dU analog (hereinafter referred as ^{Tz}dU), engineered to overcome these limitations and enable reliable DNA fluorescence imaging. Compared to its nearly nonfluorescent free form, ^{Tz}dU shows approximately a 10-fold increase in brightness in single-stranded DNA (ssDNA) and up to a 50-fold enhancement in double-stranded DNA (dsDNA). Importantly, it maintains relatively stable brightness regardless of surrounding bases by evading common quenching pathways, including solvent-induced collisional quenching and excited-state proton transfer (ESPT). The triphosphate derivative of ^{Tz}dU is efficiently utilized by various DNA polymerases, including Deep Vent and KOD XL, facilitating real-time, intensity-based monitoring of critical enzymatic processes such as PCR and primer extension without external labels. Furthermore, ^{Tz}dU can illuminate DNA in a gradient manner, enabling the visualization and encryption of information. As the first FBA to achieve universal turn-on characteristics, sequence insensitivity, and compatibility with enzymatic reactions, ^{Tz}dU serves as a novel tool for investigating nucleic acid dynamics and advancing fluorescence-based methodologies.

Received: October 14, 2025. **Revised:** June 3, 2026. **Accepted:** June 5, 2026

Graphical abstract

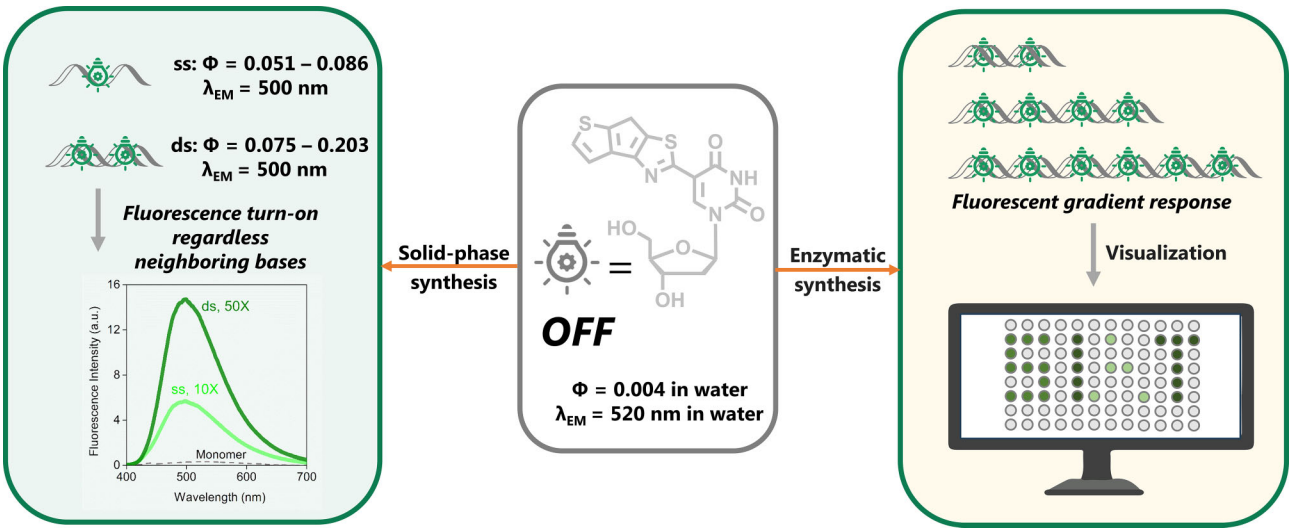

Introduction

Fluorescent nucleobase analogs (FBAs) have transformed nucleic acid research by enabling the investigation of DNA structure, dynamics, and biomolecular interactions while preserving the essential Watson–Crick base pairing properties [1–3]. These exceptional tools have significantly enhanced our capability to visualize and explore DNA at the molecular level, accelerating discoveries in fundamental biology and facilitating the development of advanced diagnostics and biosensors [4, 5]. In addition to these well-established uses, FBAs are increasingly explored in areas such as molecular information encoding, where their optical characteristics support the design of programmable molecular systems with responsive outputs [6, 7]. Such advances highlight the broader potential of FBAs in creating customizable optical platforms.

Despite their considerable utility, most FBAs suffer from severe fluorescence quenching upon incorporation into oligonucleotides (Fig. 1 and Supplementary Fig. S1). For example, 2-aminopurine (2AP), one of the most extensively studied FBAs, exhibits a 200-fold decrease in fluorescence intensity when integrated into DNA, despite exhibiting a high quantum yield (Φ = 0.6–0.7) as a free monomer [8]. Similarly, pyrrolocytosine analogs demonstrate substantial quenching when flanked by guanine, primarily due to the photoinduced electron transfer (PET) pathway [9]. The fluorescence quenching observed in most FBAs is attributed to several complex mechanisms. These include collisional deactivation of the excited state by the surrounding solvent molecules, aggregation-induced quenching resulting from a microenvironment transition, and electronic interactions such as PET or Förster resonance energy transfer (FRET) with adjacent nucleobases [10]. To address these challenges, fluorescence-maintaining FBAs such as tC, tC°, and ABN have been developed [11–13]. These analogs are capable of retaining stable fluorescence intensity regardless of their incorporation into single- (ss) or double-stranded DNA (ds-DNA), making them valuable for applications that require consistent signal output. However, their high brightness as free nucleosides can lead to undesirable background fluorescence, limiting their use in low-background detection scenarios.

A critical unmet need in this field is the development of fluorescence turn-on nucleosides—analogs that are non-fluorescent as free monomers but exhibit significant brightness enhancement upon incorporation into DNA through base stacking [14, 15]. While conventional FBAs typically suffer from severe quenching or maintain constant emission, true turn-on behavior remains a rare phenomenon. Existing approaches to developing turn-on fluorescent nucleosides can be categorized into two groups: the first conjugates an external fluorophore to the nucleoside via a non-emissive linker. A representative example is dT^{NNIR}, developed by Hocek's group: this thymidine derivative, linked to a benzylidene-tetrahydroxanthylium near-infrared dye (thiazole orange) via click chemistry, exhibits a striking 348-fold fluorescence enhancement in duplexes [16]. Notably, this approach, though effective for boosting fluorescence, is not generally classified as a true FBA; the key distinction lies in its dependence on an external fluorophore instead of an intrinsically fluorescent nucleobase.

By contrast, the second category employs intrinsically fluorescent nucleobases, such as 8-diethylamino-tC (8-DEA-tC). Relative to its free nucleoside form, 8-DEA-tC enhances fluorescence brightness by up to 5-fold, with a maximum 20-fold increase in selected duplexes [17]. Since intrinsic turn-on FBAs eliminate the need for external linkers, unlike conjugate-based systems, they offer an advantage: while conjugated systems can achieve high brightness, intrinsic turn-on FBAs provide improved structural integration by positioning the chromophore directly within the DNA helix, thus avoiding perturbations to DNA side-chain interactions. However, only few intrinsic turn-on nucleosides have been developed to date, including 5-methoxybenzofuran uridine [18], ^{DMA}T [19], and 8-DEA-tC [17]. Among these, 8-DEA-tC stands out as the most well-studied example, exhibiting sequence-dependent quenching, particularly pronounced by adjacent adenine residues. To our knowledge, no intrinsic turn-on nucleoside has successfully achieved both strong fluorescence enhancement and complete independence from neighboring base effects.

In our previous work, we developed a series of aromatic ring-conjugated thiazolyl-uracil ribonucleosides and observed distinct solvent-dependent fluorescence properties [20]. Notably, the thiophene-containing derivative exhibited a remarkable fluorescence turn-on response (35-fold enhancement) upon switching the solvent from water to methanol. This pronounced environmental sensitivity suggested that modulating

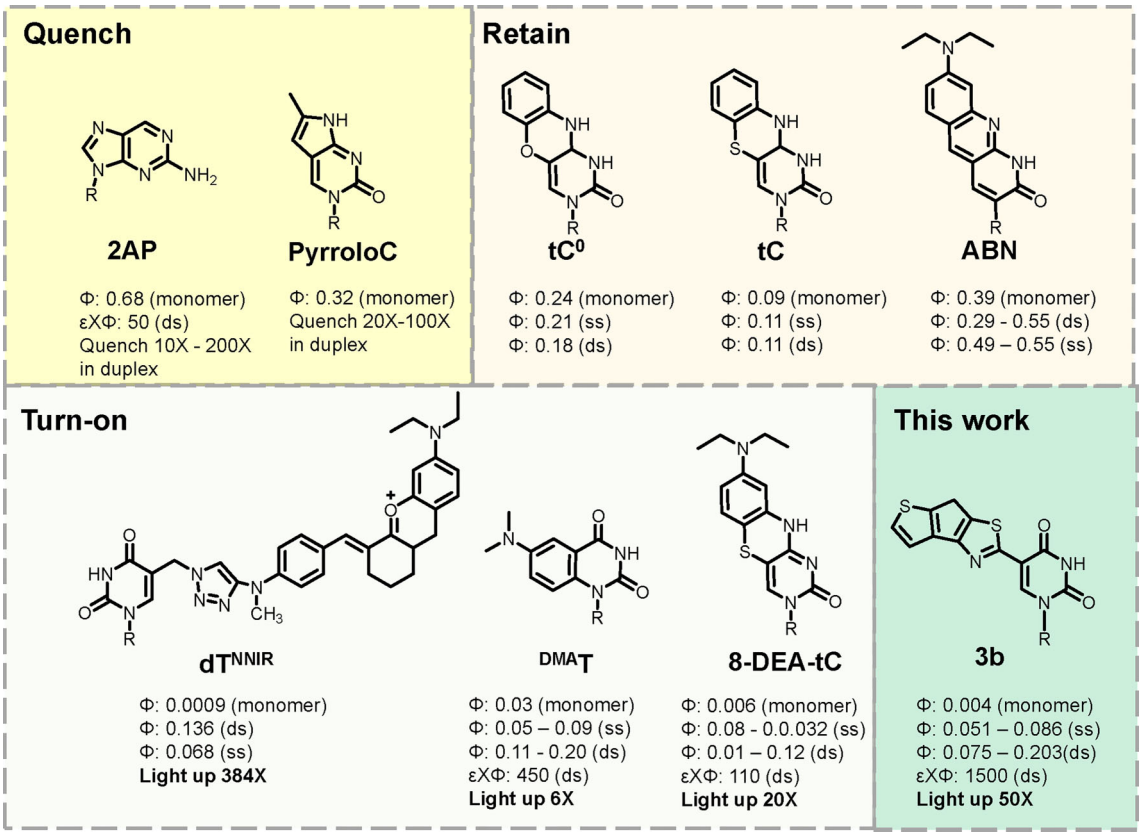

Figure 1. Structures of three types of fluorescent nucleosides and our work. The average brightness and quantum yield of FBAs over various DNA sequence were listed.

the local microenvironment could induce a fluorescence turn-on effect, an approach analogous to that employed by previously reported DNA turn-on probes such as 8-DEA-tC. To extend this concept to DNA-based systems, we designed and synthesized the corresponding 2′-deoxyuridine derivatives bearing either a phenyl (3a) or thiophene (3b, ^{Tz}dU) substituent, and systematically characterized their photophysical properties upon incorporation into DNA oligonucleotides. The thiophene moiety in ^{Tz}dU was anticipated to confer enhanced environmental sensitivity, attributed to its reduced aromaticity and potential for specific solvent interactions. Consistent with this expectation, ^{Tz}dU displayed robust turn-on fluorescence in both ssDNA and dsDNA, while remaining largely sequence-insensitive. Subsequent mechanistic studies revealed that this key photophysical distinction arises from a combination of solvent shielding and distinct excited-state dynamics imparted by the thiophene ring—specifically, enhanced susceptibility to excited-state proton transfer (ESPT) in aqueous solution and effective suppression of guanine-mediated PET. Together, these effects ultimately give rise to the pronounced fluorescence enhancement observed for ^{Tz}dU in polynucleotide environments. The successful incorporation of ^{Tz}dU triphosphate by DNA polymerases in primer extension (PEX) experiments and polymerase chain reactions (PCRs) underscores its potential for fluorescence-based DNA sensing studies. Notably, the fluorescence intensity of ^{Tz}dU in duplex is proportional to the number of incorporated residues, demonstrating a clear gradient in its turn-on response. Such programmable fluorescence output further suggests broader applicability in molecular encryption and information encoding, where intensity-based signaling could be used to augment sequence-based data interpretation. Collectively, our work presents the development of a sequence-insensitive turn-on fluorescent nucleoside for DNA detection and illumination, expanding the scope for fundamental studies and practical applications of FBAs.

Materials and methods

Material and instrumentation

All chemicals and solvents were of laboratory grade, obtained from commercial suppliers, and used without further purification. Thin-layer chromatography (TLC) was performed on aluminum sheets pre-coated with silica gel 60 F254. Flash column chromatography (FC) was performed on silica gel 60 under 0.4 bar pressure. UV–vis spectra were recorded on a U-3200 UV-vis spectrometer (Meipuda, China). ^{1}H, ^{13}C, and ^{31}P NMR spectra were acquired on Bruker spectrometers operating at 400 MHz or 500 MHz for ^{1}H, 100 MHz for ^{13}C, and 121.52 MHz for ^{31}P. Chemical shifts (δ) are reported in parts per million (ppm) relative to tetramethylsilane (MeSi) as the internal standard for ^{1}H and ^{13}C NMR, and relative to external 85% H_3PO for ^{31}P NMR. Coupling constants (*J*) are reported in Hertz (Hz). For spectra recorded in DMSO-d_6, the solvent residual peak was referenced to 2.50 ppm for ^{1}H NMR and 39.50 ppm for ^{13}C NMR.

Thermal melting curves were measured using a Cary3500 UV/Vis spectrophotometer (Agilent) equipped with a thermoelectrically controlled cell holder. The temperature in the reference cell was monitored continuously with a Pt-100 resis-

tor, with a heating rate of 1°C min^{-1}. Thermodynamic data were calculated using the program MeltWin (version 3.0) by curve fitting of the melting profiles according to a two-state model.

Chemical synthesis

5-Cyano-1-(2-deoxy-3,5-*O*-di-acetyl-β-d-erythro-pentofuranosyl)-uracil (1)

To a solution of 2′-deoxyuridine (5.0 g, 21.9 mmol), DMAP (268 mg, 0.1 eq.), and triethylamine (6.7 g, 65.7 mmol, 3.0 eq.) in CH_3CN (80 ml) was added acetic anhydride (5.6 g, 54.8 mmol, 2.5 eq.). After stirring for 30 min, the reaction was quenched with MeOH (10 ml) and stirred for an additional 10 min. The mixture was concentrated *in vacuo*, and the residue was extracted with CH_2Cl_2 (2 × 80 ml). The combined organic layers were washed with brine (3 × 100 ml), dried over MgSO, and concentrated *in vacuo*. The resulting colorless foam (6.5 g, 20.8 mmol, 95%) was redissolved in CH_3CN (70 ml). I_2 (3.2 g, 12.5 mmol, 0.6 eq.) and CAN (5.5 g, 10.4 mmol, 0.5 eq.) were added, and the mixture was stirred at 80°C for 1 h. After cooling to room temperature, the solvents were evaporated *in vacuo*. The dark oily residue was dissolved in EtOAc (150 ml) and washed with aqueous $Na_2S_2O_3$ solution (100 ml). The organic layer was washed with saturated NaCl solution (150 ml), dried over MgSO, and concentrated *in vacuo* to afford the 5-iodo product as a white solid (8.7 g, 19.9 mmol, 95%).

The solid was dissolved in pyridine (70 ml), and HMDS (25 ml, 119.4 mmol, 6.0 eq.) was added. The mixture was stirred at room temperature for 12 h under Ar. Pyridine was removed *in vacuo*, and the resulting colorless oil was redissolved in dry pyridine (100 ml). CuCN (10.7 g, 119.4 mmol, 6.0 eq.) was added, and the solution was heated to 120°C under Ar for 6 h. After cooling to room temperature, pyridine was removed *in vacuo*. The residue was taken up in EtOAc (200 ml), filtered through a pad of Celite®, and washed extensively with EtOAc. The combined filtrate and washings were washed with brine (2 × 125 ml), dried over Na_2SO, and concentrated *in vacuo*. The resulting light gray foam (6.4 g, 87% yield over three steps) was used directly in the next reaction without purification.

^{1}H NMR (400 MHz, DMSO-d_6) δ 12.11 (s, 1H), 8.59 (s, 1H), 6.08 (t, J = 6.7 Hz, 1H), 5.20 (dt, J = 6.9, 3.3 Hz, 1H), 4.32–4.19 (m, 3H), 2.58–2.51 (m, 1H), 2.40 (ddd, J = 14.5, 6.4, 3.3 Hz, 1H), 2.06 (d, J = 1.6 Hz, 6H); ^{13}C{^{1}H} NMR (100 MHz, DMSO) δ 170.1, 170.0, 160.0, 149.8, 148.9, 114.2, 88.7, 86.0, 81.8, 73.3, 63.4, 36.5, 20.7, 20.5;

HR-ESIMS (*m/z*): [M − H$^-$] calcd for $C_{14}H_{14}N_3O_7$ − 336.0837, found 336.0837.

5-Carbothioamide-1-(2-deoxy-3,5-*O*-di-acetyl-β-D-erythro-pentofuranosyl)-uracil (2)

To a solution of compound 1 (2.0 g, 6.0 mmol) in *N*,*N*-dimethylformamide (DMF) (16 ml) were added 70% aqueous NaSH (1.44 g, 18 mmol, 3.0 eq.), $Et_2NH{\cdot}HCl$ (2.97 g, 27 mmol, 4.5 eq.), pyridine (1.5 ml, 18 mmol, 3.0 eq.), and H_2O (4 ml). The reaction mixture was stirred under Ar at 80°C for 3 h. The resulting solution was poured into brine (70 ml, 2 M) and extracted with EtOAc (3 × 40 ml). The combined organic layers were washed with saturated aqueous NaCl solution (1 × 50 ml), dried over MgSO, filtered, and concentrated *in vacuo*. The crude yellow solid was triturated with EtOAc (15 ml) to afford protected nucleoside 2 (1.6 g, 73%) as a yellow solid.

^{1}NMR (400 MHz, DMSO-d_6) δ 12.05 (s, 1H), 10.21 (d, J = 4.4 Hz, 1H), 9.91 (d, J = 4.4 Hz, 1H), 9.15 (s, 1H), 6.11 (t, J = 6.8 Hz, 1H), 5.22 (dt, J = 6.6, 2.4 Hz, 1H), 4.43–4.35 (m, 1H), 4.21 (d, J = 3.9 Hz, 2H), 2.53 (d, J = 2.2 Hz, 1H), 2.41 (dt, J = 14.3, 6.8 Hz, 1H), 2.07 (d, J = 8.9 Hz, 6H); ^{13}C{^{1}H}NMR (100 MHz, DMSO) δ 191.43, 170.16, 170.00, 162.56, 149.61, 148.97, 109.16, 86.62, 82.36, 74.20, 63.72, 37.65, 20.80, 20.74.

HR-ESI MS (m/z): [M + Na^+] calcd for $C_{14}H_{18}N_3O_7S\,Na^+$ 394.0679, found 394.0679.

5-(8H-indeno[1,2-d]thiazol-2-yl)-1-(2-deoxy-β-D-erythro-pentofuranosyl)-uracil (3a)

2-Bromo-1-indanone (815 mg, 3.8 mmol, 1.4 eq.) was added to a solution of compound 2 (1 g, 2.7 mmol) in DMF (10 ml). The reaction mixture was stirred at 105°C for 1 h using an oil bath. After cooling, the mixture was poured into H_2O (50 ml). The resulting yellow precipitate was collected by filtration, washed thoroughly with H_2O, and dried. The solid was dissolved in a mixture of EtOH/H_2O (4:1, v/v; 20 ml), and NaOH (216 mg, 5.4 mmol, 2.0 eq.) was added. The solution was stirred at room temperature for 30 min. The reaction mixture was carefully neutralized with aqueous AcOH (10% v/v) and concentrated *in vacuo*. The crude yellow solid was triturated with H_2O (15 ml), collected by filtration, and washed with EtOAc (10 ml) to afford nucleoside 3a (880 mg, 82%) as a white solid.

^{1}H NMR (400 MHz, DMSO-*d6*) δ 11.95 (s, 1H), 9.01 (s, 1H), 7.73 (d, J = 7.4 Hz, 1H), 7.56 (d, J = 7.5 Hz, 1H), 7.39 (t, J = 7.4 Hz, 1H), 7.26 (t, J = 7.5 Hz, 1H), 6.23 (t, J = 6.5 Hz, 1H), 5.35 (d, J = 4.3 Hz, 1H), 5.15 (t, J = 4.7 Hz, 1H), 4.33 (t, J = 3.8 Hz, 1H), 3.94 (s, 2H), 3.92–3.89 (m, 1H), 3.74–3.64 (m, 2H), 2.27 (t, J = 5.7 Hz, 2H).

^{13}C{^{1}H} NMR (100 MHz, DMSO-d_6) δ 162.3, 161.2, 159.9, 149.2, 146.4, 138.8, 137.1, 136.5, 126.8, 125.3, 125.3, 118.6, 107.9, 87.8, 85.5, 70.3, 61.1, 40.4, 32.2.

HR-ESI MS (*m/z*): [M + H$^+$] calcd for $C_{19}H_{18}N_3O_5S^+$ 400.0962, found 400.0962.

5-(4H-thieno[2′,3′:4,5]cyclopenta[1,2-d]thiazol-2-yl)-1-(2-deoxy-β-D-erythro-pentofuranosyl)-uracil (3b, TzdU)

Following the procedure described for 3a, but using 5-bromo-5,6-dihydro-4H-cyclopenta[b]thiophen-4-one (7b) as the starting material, 3b was obtained as a yellow solid.

^{1}H NMR (500 MHz, DMSO-d_6) δ 8.89 (s, 1H), 7.63 (d, J = 5.0 Hz, 1H), 7.33 (d, J = 4.9 Hz, 1H), 6.23 (t, J = 6.6 Hz, 1H), 5.33 (s, 1H), 5.10 (s, 1H), 4.31 (q, J = 4.3 Hz, 1H), 3.98 (s, 2H), 3.89 (q, J = 3.7 Hz, 1H), 3.66 (qd, J = 11.6, 3.8 Hz, 2H), 2.29–2.21 (m, 2H).

^{13}C{^{1}H} NMR (150 MHz, DMSO-d6) δ 161.19, 160.63, 156.46, 149.08, 144.92, 141.20, 137.67, 136.35, 128.52, 117.16, 107.59, 87.20, 84.90, 69.82, 60.65, 39.75, 30.54.

HR-ESI MS (*m/z*): [M + H$^+$] calcd for $C_{17}H_{16}N_3O_5S_2^+$ 406.0526, found 406.0521.

5-(8H-indeno[1,2-d]thiazol-2-yl)-1-(2-deoxy-β-D-erythro-pentofuranosyl)-5-(triisopropylsilylethynyl)-uracil (4a)

Compound 3a (250 mg, 0.63 mmol) was coevaporated with pyridine (2 × 2.5 ml) to dryness. The residue was dissolved in dry pyridine (8 ml), and 4,4′-dimethoxytrityl chloride (DMT-Cl) (278 mg, 0.82 mmol, 1.3 eq.) was added. The reaction mixture was stirred at room temperature for 18 h. The solution was concentrated *in vacuo* and purified by flash column chromatography (silica gel; gradient elution CH_2Cl_2/MeOH, 50:1 v/v) to afford compound 4a (290 mg, 66%) as a white solid.

^{1}H NMR (500 MHz, DMSO-d_6) δ 12.05 (s, 1H), 8.73 (s, 1H), 7.52 (d, J = 6.4 Hz, 1H), 7.42 (d, J = 7.5 Hz, 2H), 7.33–7.26 (m, 4H), 7.21 (dd, J = 9.4, 6.4 Hz, 4H), 7.12 (t, J = 7.4 Hz, 1H), 7.05–6.96 (m, 1H), 6.82–6.66 (m, 4H), 6.17 (t, J = 6.4 Hz, 1H), 5.37 (d, J = 4.3 Hz, 1H), 4.18–4.12 (m, 1H), 4.05 (q, J = 3.9 Hz, 1H), 3.92 (s, 2H), 3.58 (d, J = 7.3 Hz, 6H), 3.35–3.32 (m, 1H), 3.24 (dd, J = 10.6, 4.9 Hz, 1H), 2.38–2.32(m, 1H), 2.29–2.21 (m, 1H).

^{13}C{^{1}H} NMR (125 MHz, DMSO-d_6) δ 162.53, 161.77, 160.47, 158.44, 158.39, 149.57, 146.74, 145.18, 138.34, 137.55, 136.84, 135.92, 135.86, 130.21, 130.08, 128.19, 128.16, 127.06, 125.62, 125.53, 119.05, 113.52, 108.30, 86.76, 86.39, 71.01, 63.97, 55.27, 40.99, 32.59.

HR-ESI MS (*m/z*): [M + H$^+$] calcd for $C_{40}H_{36}N_3O_7S^+$ 702.2268, found 702.2267.

5-(4H-thieno[2′,3′:4,5]cyclopenta[1,2-d]thiazol-2-yl)-1-(2-deoxy-β-D-erythro-pentofuranosyl)-5′-(triisopropylsilylethynyl)-uracil (4b)

Following the procedure described for 4a, compound 4b was prepared from nucleoside 3b (250 mg, 0.62 mmol) to afford 4b as a white solid (300 mg, 69%).

^{1}H NMR (600 MHz, DMSO-d_6) δ 11.99 (s, 1H), 8.66 (s, 1H), 7.46 (d, J = 5.0 Hz, 1H), 7.39 (d, J = 7.3 Hz, 2H), 7.27 (t, J = 9.3 Hz, 4H), 7.18 (t, J = 7.6 Hz, 2H), 7.09 (t, J = 7.3 Hz, 1H), 6.71 (dd, J = 11.5, 8.9 Hz, 4H), 6.66 (d, J = 5.0 Hz, 1H), 6.14 (t, J = 6.4 Hz, 1H), 5.33 (d, J = 4.4 Hz, 1H), 4.15 (dd, J = 6.4, 3.6 Hz, 1H), 3.99 (q, J = 3.8 Hz, 1H), 3.91 (s, 2H), 3.57 (d, J = 8.3 Hz, 6H), 3.29–3.19 (m, 2H), 2.34–2.22 (m, 2H).

^{13}C{^{1}H}NMR (126 MHz, DMSO-d_6) δ 161.24, 160.53, 157.94, 157.88, 157.01, 149.07, 145.23, 144.69, 141.60, 137.42, 136.91, 135.53, 135.38, 129.76, 129.55, 128.53, 127.69, 126.56, 117.62, 113.03, 108.01, 86.20, 85.91, 70.48, 63.41, 54.78, 54.76, 40.50, 30.91.

HR-ESI MS (*m/z*): [M + H$^+$] calcd for $C_{38}H_{34}N_3O_7S_2^+$ 708.1833, found 708.1826.

3′-Cyanoethyldiisopropylphosphoramidite (5a)

Compound 4a (205 mg, 0.29 mmol) was coevaporated with toluene (2 × 3 ml) to dryness. The residue was dissolved in dry CH_2Cl_2 (5 ml) under an inert atmosphere. To the stirred solution was added *N,N*-diisopropylethylamine (DIPEA; 113 mg, 0.15 ml, 0.88 mmol, 3.0 eq.) followed by 2-cyanoethyl *N,N*-diisopropylchlorophosphoramidite (89 mg, 0.38 mmol, 1.3 eq.). After stirring at room temperature for 20 min, the reaction mixture was diluted with CH_2Cl_2 (30 ml) and washed with 5% aqueous $NaHCO_3$ solution (20 ml). The organic layer was dried over Na_2SO, filtered, and concentrated *in vacuo*. The residue was purified by flash column chromatography (silica gel; hexane/EtOAc, 1:1 v/v) to afford phosphoramidite 5a (223 mg, 85%) as a white solid.

^{1}H NMR (500 MHz, DMSO-d_6) δ 12.05 (s, 1H), 8.76 (d, J = 15.3 Hz, 1H), 7.57–7.49 (m, 1H), 7.46–7.38 (m, 2H), 7.33–7.26 (m, 4H), 7.24–7.11 (m, 5H), 7.04–6.99 (m, 1H), 6.80–6.68 (m, 4H), 6.19 (dt, J = 13.0, 6.4 Hz, 1H), 4.46–4.36 (m, 1H), 4.18 (dq, J = 21.0, 3.9 Hz, 1H), 3.92 (d, J = 3.1 Hz, 2H), 3.79–3.68 (m, 1H), 3.64–3.47 (m, 9H), 3.42 (ddd, J = 29.8, 10.7, 3.4 Hz, 1H), 3.30–3.24 (m, 1H), 2.77 (t, J = 5.9 Hz, 1H), 2.66 (td, J = 5.8, 1.8 Hz, 1H), 2.50–2.38 (m, 2H), 1.18–1.07 (m, 9H), 1.01 (d, J = 6.7 Hz, 3H).

^{31}P NMR (202 MHz, DMSO-d_6) δ 147.56, 147.41.

HR-ESI MS (*m/z*): [M + H$^+$] calcd for $C_{49}H_{53}N_5O_8PS^+$ 902.3347, found 902.3346.

3′-Cyanoethyldiisopropylphosphoramidite (5b)

Following the procedure described for 5a, compound 5b was prepared from 4b to afford 5b as a yellow foam (280 mg, 88%).

^{1}H NMR (400 MHz, DMSO-d_6) δ 12.04 (s, 1H), 8.71 (d, J = 10.4 Hz, 1H), 7.48 (t, J = 5.7 Hz, 1H), 7.41 (dd, J = 7.7, 4.5 Hz, 2H), 7.33–7.25 (m, 4H), 7.19 (t, J = 7.6 Hz, 2H), 7.12 (t, J = 7.3 Hz, 1H), 6.78–6.63 (m, 5H), 6.17 (dt, J = 12.0, 6.3 Hz, 1H), 4.40 (s, 1H), 4.20–4.10 (m, 1H), 3.97–3.90 (m, 2H), 3.72 (t, J = 8.8 Hz, 1H), 3.64–3.54 (m, 8H), 3.51 (ddd, J = 9.9, 6.7, 3.4 Hz, 1H), 3.33 (s, 1H), 3.28–3.23 (m, 1H), 2.76 (t, J = 5.9 Hz, 1H), 2.66 (d, J = 6.0 Hz, 1H), 2.45 (t, J = 5.6 Hz, 2H), 1.16–1.07 (m, 9H), 1.00 (d, J = 6.7 Hz, 3H).

^{31}P NMR (200 MHz, DMSO-d_6) δ 147.42, 147.30.

HR-ESI MS (*m/z*): [M + H$^+$] calcd for $C_{47}H_{51}N_5O_8PS_2^+$908.2911, found 908.2910.

3a triphosphate (6a)

Compound 3a (30 mg, 0.075 mmol) was coevaporated with anhydrous pyridine (2 × 2 ml) to dryness. The residue was dissolved in dry trimethyl phosphate (1.5 ml) under N_2. To the stirred solution at 0°C was added freshly distilled $POCl_3$ (11.2 µl, 0.12 mmol, 1.6 eq.). The mixture was stirred for 2 h at 0°C. A solution of tributylammonium pyrophosphate (0.5 M in DMF, 1.5 ml, 0.75 mmol, 10 eq.) and tributylamine (168 µl, 0.75 mmol, 10 eq.) was added in one portion. The ice bath was removed, and stirring continued at room temperature for 30 min. The reaction was quenched with 2 M TEAB buffer (pH 8.0, 15 ml), and extracted with CH_2Cl_2 (4 × 5 ml). The aqueous layer was concentrated *in vacuo* to ~5 ml and purified by reversed-phase flash chromatography (C18 column; linear gradient: 0 → 40% CH_3CN in 50 mM TEAB (pH 8.0) over 30 min). Product-containing fractions were lyophilized to afford the title triphosphate as a tetratriethylammonium salt (white foam, 30 mg, 43%).

^{1}H NMR (500 MHz, DMSO-d_6) δ 8.63 (s, 1H), 7.87 (d, J = 7.5 Hz, 1H), 7.56 (d, J = 7.4 Hz, 1H), 7.38 (t, J = 7.5 Hz, 1H), 7.26 (t, J = 7.5 Hz, 1H), 6.16 (t, J = 6.5 Hz, 1H), 4.35 (dt, J = 6.6, 3.7 Hz, 1H), 4.06 (d, J = 7.2 Hz, 3H), 3.95 (s, 2H), 2.37–2.15 (m, 2H).

^{31}P NMR (202 MHz, DMSO-d_6) δ -11.27, -11.38, -12.17, -12.29, -23.90, -24.01, -24.13.

HR-ESI MS (*m/z*): [M-H$^-$] calcd for $C_{19}H_{19}N_3O_{14}P_3S^-$ 637.9806, found 637.9800.

3b triphosphate (6b)

Following the procedure described for 6a, compound 6b was prepared from 3b to afford 6b as a yellow foam (45 mg, 64%).

^{1}H NMR (500 MHz, DMSO-d_6) δ 8.58 (s, 1H), 7.58 (d, J = 4.9 Hz, 1H), 7.49 (d, J = 5.0 Hz, 1H), 6.15 (t, J = 6.5 Hz, 1H), 4.34 (dt, J = 6.6, 3.8 Hz, 1H), 4.04 (d, J = 7.1 Hz, 3H), 3.98 (s, 2H), 2.39–2.14 (m, 2H);

^{31}P NMR (202 MHz, DMSO-d_6) δ -11.29, -11.40, -12.21, -12.33, -23.93, -24.05, -24.17;

HR-ESI MS (*m/z*): [M-H$^-$] calcd for $C_{17}H_{17}N_3O_{14}P_3S_2^-$ 643.9370, found 643.9378.

Photophysical properties of fluorescent nucleosides

For all photophysical experiments, fluorescent nucleosides 3a–b were prepared as stock solutions in DMSO and stored at –20°C. Measurements were performed using spectrophotometric-grade 1,4-dioxane, DMSO, ethanol, methanol, and deionized H_2O. Final DMSO concentrations were kept below 0.1% (v/v) in all assays.

Density function theory computations

Molecular geometries were optimized and thermal corrections were calculated using density functional theory (DFT) with the B3LYP functional and 6–31 + G(d) basis set. Calculations were employed the conductor-like polarizable continuum model (C-PCM) for aqueous solvation at 298.15 K. The absence of imaginary frequencies confirmed that all structures were at local minima. All computations were performed using Gaussian 16 (Revision C.01).

Oligonucleotide synthesis and characterization

Oligonucleotides were synthesized on ABI 392-08 synthesizer using standard phosphoramidite chemistry and modified building blocks 5a or 5b, following the manufacturer's protocol for 3′-cyanoethyl phosphoramidites. Synthesized oligonucleotides were purified by high-performance liquid chromatography (HPLC). Molecular masses were verified by matrix-assisted laser desorption/ionization time-of-flight mass spectrometry (MALDI-TOF MS) in the linear negative mode with 3-hydroxypicolinic acid (3-HPA) as a matrix.

Melting temperature analysis (T_m)

Hybridization and UV melting experiments were performed in a buffer containing 0.1 M NaCl, 10 mM $MgCl_2$, and 10 mM sodium cacodylate (pH 7.0) using a Cary 3500 UV-Vis spectrometer (Agilent, USA). Temperature was cycled from 20°C to 80°C at 0.6°C/min (heating) and from 80°C to 20°C at 0.6°C/min (cooling), with absorbance measured at 260 nm every 0.6°C.

Primer extension reaction

Typically, a 20-μl reaction was set up in a PCR tube, the DNA template, primer, natural dNTPs, 6a or 6b, Deep vent DNA polymerase or KOD XL DNA polymerase were mixed in 1× polymerase buffer and incubated at 60°C for 60 min. The reaction was stopped by heating at 95°C for 5 min. The reaction mixture was treated according to the requirement of following investigation.

Data visualization experiment

In the fluorescence intensity-based DNA visualization experiments, pre-designed patterns were projected onto a 12 × 8 grid corresponding directly to a 96-well microplate layout. Fluorescence intensities were mapped to distinct pixel brightness levels within a color scale. To maximize contrast, PEX products exhibiting significant intensity differentials were selected: PEX product 1 (lowest intensity) was assigned the darkest shade, product 3 (medium intensity) was assigned as a mid-range brightness, and product 6 (highest intensity) was assigned as the brightest shade. For proof-of-concept validation, two patterns ("2025" and a face) were designed. The selected PEX products were dispensed into their designated wells within the 96-well microplates, successfully generating the target patterns upon projection. For key encryption assays, unlabeled PEX products were diluted in the sodium cacodylate buffered solution (pH 7.0) and loaded into the opaque 96-well microplates according to the pre-designed pattern layout and analyzed by the microplate reader with excitation at 375 nm and emission collected at 510 nm. The collected intensity data were mapped to preset numerical values which were further converted to heatmaps to display the pre-designed patterns.

Chinese poem encryption and decryption

The poem was encrypted using the preconfigured numerical key "13 452" via the Blowfish cryptographic algorithm (http://tool.chacuo.net/cryptblowfish), generating the cipher text which was converted to DNA sequences using a web-based encoding platform (http://storage.dailab.xyz:16666/codec). Three 500-nucleotide DNA sequences and associated primers were generated. Each DNA construct was individually cloned into separate plasmid vectors (pUC57-Kan+), transformed into distinct *Escherichia coli* strains (DH5α), and amplified over ≥2000 generations. Plasmids were subsequently purified from cultured transformants and used as PCR templates to recover the original DNA sequences. Sanger sequencing of the amplicons and the results were subjected to decryption algorithm and achieved recovery of the original poem.

Results

Synthesis of fluorescent nucleosides 3a and 3b

We developed an optimized synthetic route for fluorescent nucleosides 3a and 3b, improving upon our previous thiazolyluridine chemistry [20]. This method uses commercially available 2′-deoxyuridine and offers three key advantages: elimination of chromatographic purification, enhanced safety, and high yields.

The synthesis features a safer NaHS-based protocol to convert cyano precursor 1 [21, 22] into thioamide intermediate 2 (77% yield), avoiding hazardous H_2S release (Scheme 1). Intermediate 2 enables diverse Hantzsch reactions with aromatic α-bromocarbonyl compounds, followed by simple deacetylation. The entire seven-step process to 3a (55% overall yield) and 3b (52% overall yield) proceeds without column chromatography—only trituration or direct solid handling is needed. All compounds were fully characterized by NMR and HRMS, and successfully converted into phosphoramidites and triphosphates for oligonucleotide synthesis and enzymatic studies. This efficient, scalable, and safer method-

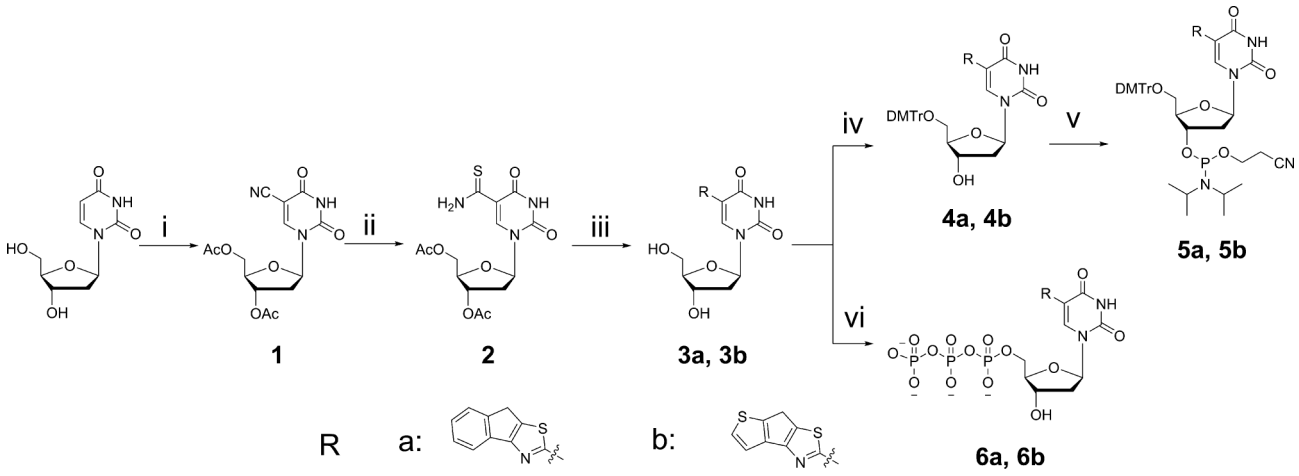

Scheme 1. Scheme for the synthesis of FBAs 3a and 3b and their conversion into phosphoramidites and triphosphates. Reagents and conditions: (i) Triethylamine, 4-dimethylaminopyridine, acetic anhydride, acetonitrile; Ammonium ceric sulfate, iodine, acetonitrile, 80°C; 1,1,1,3,3,3-Hexamethyldisilazane, pyridine; copper(I) cyanide, pyridine; (ii) Sodium hydrosulfide, diethylamine hydrochloride, pyridine, water, dimethylformamide, N_2, 80°C, 5 h; (iii) Aromatic α-bromocarbonyl compounds, dimethylformamide, 105°C, 0.5 h; (iv) 4,4′-dimethoxytrityl chloride, pyridine, 25°C, 18 h; (v) 2-cyano ethyl *N,N*-diisopropylchlorophosphoroamidite, *N,N*-diisopropylethylamine, dichloromethane, N_2, 25°C, 20 min; (vi) Phosphorus oxychloride, trimethylphosphate, N_2, 0°C, 2 h; tributylammonium pyrophosphate (0.5 M in dimethylformamide), tributylamine, 25°C, 20 min; 2 M triethylammonium bicarbonate buffer.

ology significantly expands access to fluorescent DNA probes for nucleic acid research.

Photophysical characterization of nucleosides 3a and 3b

With fluorescent nucleosides in hand, we began by measuring the photophysical characteristics of 3a and 3b (^{Tz}dU) in various solvents with differing polarities, pH levels, and viscosities. Initially, we assessed the fluorescence emission of 3b across a range of solvents. The results indicated that 3b exhibited solvent-dependent fluorescence, with significant quenching observed in water while retaining its emission in organic solvents, with the strongest emission recorded in dimethyl sulfoxide (DMSO) (Fig. 2A, and Supplementary Tables S1 and S2). In-depth analysis revealed that in aprotic solvents, the fluorescence emission intensity of 3b increases with solvent polarity, accompanied by a noticeable redshift in the emission peak. In contrast, in protic solvents, the emission intensity decreases with increasing solvent polarity, though the emission peak continues to redshift with polarity. A further correlation plot of the Stokes shift against Reichardt's E^T_{30} parameter across solvents of varying polarity showed a nearly linear relationship for 3b (Fig. 2B and Supplementary Fig. S3), suggesting the presence of intramolecular charge transfer (ICT) characteristics [22].

Additionally, considering that pH can influence the fluorescence emission of fluorescent molecules, we investigated the impact of pH on 3b's fluorescence. Our findings revealed that3b demonstrated a pH-dependent fluorescence trait, with greater quenching occurring in more acidic environments (Fig. 2C and Supplementary Fig. S5). Based on the foregoing discussion, 3b possesses an ICT character, these results indicated that a more acidic environment significantly enhance the ICT process, thereby strongly suppressing the fluorescence emission intensity of 3b. The turn-on properties of fluorescent nucleosides are highly dependent on their surrounding environment, therefore, we further measured the fluorescence emission of 3b in solvents of different viscosities (Supplementary Tables S3 and S4). Given the similar polarity yet distinct viscosities of methanol and glycerol, we prepared solvent systems with continuously tunable viscosity by blending the two components at varying ratios. However, no clear correlation was observed between the fluorescence emission of 3b and solvent viscosity in a Förster–Hoffmann plot (Fig. 2D and E), indicating that it does not behave as a molecular rotor.

For comparison, we also measured the fluorescence quantum yields of 3a. Similar to most microenvironment-sensitive fluorescent nucleosides [23–25], 3a exhibited negligible variation in quantum yields across diverse solvents (Φem = 0.14–0.25), whereas 3b displayed significant quenching in water (Fig. 2F, and Supplementary Figs S2 and S4). These characteristics suggest that 3b is an optimal candidate for a turn-on fluorescent nucleoside.

Fluorescent turn-on properties of 3a and 3b in oligonucleotides

To evaluate the potential of 3b for sensing and visuallization applications, we systematically investigated its fluorescence behavior upon incorporation into DNA strands, as many fluorescent nucleosides undergo quenching by adjacent bases. Utilizing solid-phase DNA synthesis, we incorporated both 3a and 3b (via phosphoramidites 5a and 5b) into the model sequence ACTCAX$_1$3X$_2$GCGCT, examining various combinations of neighboring bases (Table 1, and Supplementary Tables S6 and S7). Importantly, both analogs demonstrated excellent structural compatibility with duplex formation, as confirmed by circular dichroism (CD) spectroscopy (Supplementary Figs S9–S12), which showed preserved B-form geometry and minimal thermal destabilization (ΔT_m = 3–4°C, Supplementary Table S8) [10, 26, 27].

Detailed quantum yield measurements revealed striking differences between the two analogs. For 3a, we observed significant sequence-dependent fluorescence variations (Φem = 0.04–0.44) in ssDNA (Fig. 3A and Supplementary Table S9). The fluorescence was particularly sensitive to adja-

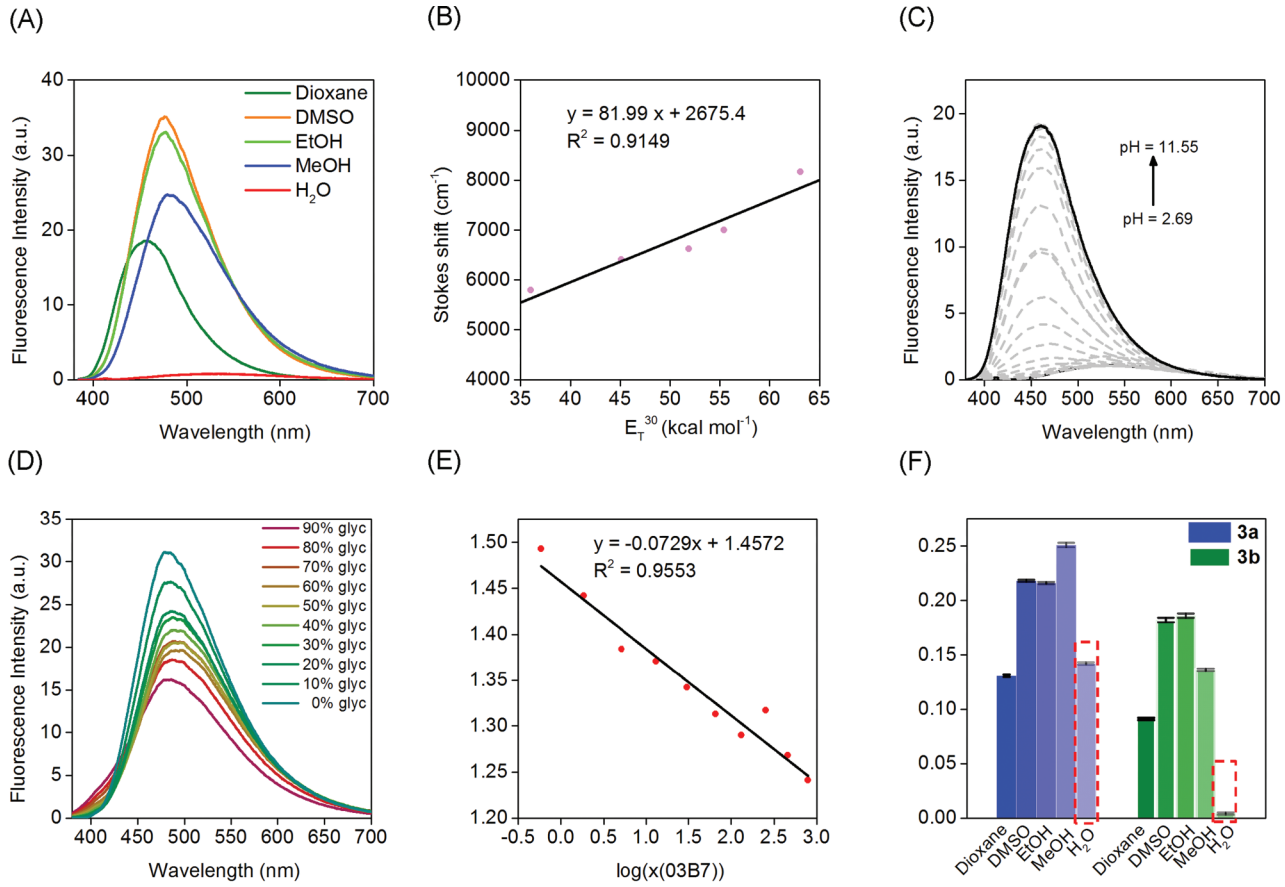

Figure 2. Characterization of compounds 3a and 3b. (**A**) Fluorescence spectra of 3b in different solvents. (**B**) Stokes shift in fluorescence spectra of 3b in different solvents. (**C**) 3b's fluorescence dependence on pH. (**D**) 3b's fluorescence dependence on viscosity. (**E**) The Förster–Hoffmann fitting of 3b against viscosity. (**F**) Fluorescence quantum yields of 3a and 3b in different solvents.

Table 1. The photophysical properties of 3b-incorporated oligonucleotides[a]

Sequence Name[b]	λ_{ex} (nm) ss/ds	ε ($cm^{-1}M^{-1}$) ss(ds)	λ_{em} (nm) ss (ds)	Φ ss (ds)	$\varepsilon \times \Phi$ ($cm^{-1}M^{-1}$) ss (ds)	$T_m/\Delta T_m$ (°C)
AA-3b	375 (375)	10 400 (11 300)	500 (500)	0.073 (0.104)	759 (1175)	52.7/-2.8
AT-3b	376 (376)	11 800 (12 300)	501 (500)	0.068 (0.174)	802 (2140)	53.7/-3.7
TT -3b	373 (375)	12 000 (11 600)	497 (500)	0.067 (0.203)	800 (2360)	54.4/-2.8
TG-3b	371 (372)	11 300 (10 300)	498 (500)	0.069 (0.165)	780 (1700)	58.8/-2.4
TC-3b	373 (374)	11 100 (11 200)	498 (499)	0.051 (0.143)	566 (1602)	57.0/-3.6
GG-3b	373 (372)	11 600 (10 600)	500 (498)	0.053 (0.115)	615 (1219)	59.8/-2.7
GA-3b	373 (373)	11 000 (11 200)	500 (500)	0.063 (0.075)	693 (840)	55.9/-2.1
GC-3b	375 (374)	11 100 (10 000)	500 (499)	0.063 (0.105)	699 (1050)	60.5/-3.2
CC-3b	374 (373)	10 700 (11 200)	498 (497)	0.064 (0.146)	685 (1635)	62.5/-1.4
CA-3b	375 (372)	10 300 (11 200)	499 (499)	0.086 (0.097)	886 (1086)	57.1/-2.6
ACC-3b	376 (373)	10 400 (10 400)	500 (500)	0.066 (0.130)	686 (1352)	56.2/+0.7
3b	365	9100	520	0.004	36	

[a]More details for photophysical measurements were given in the Supporting Information. All measurements were performed at 25°C in the buffer containing 0.1 M NaCl, 10 mM $MgCl_2$, 10 mM Na-cacodylate, pH 7.0. Final concentration of all oligonucleotides was adjusted to 1.5 μM. [b]Sequences named after neighboring bases, e.g. 5′-d(ACTCAX3bYGCCGT)-3′(sequence name AA-3b: X = Y = A).

cent guanine residues, showing 3.4-fold quenching in single strands and 5.7-fold quenching in duplexes (Fig. 3C and Supplementary Fig. S13). This quenching behavior is attributed to PET from guanine (with its high reduction potential). However, 3a achieved remarkable brightness (~6000 M^{-1} cm^{-1}) in favorable sequence contexts (AA, TT, and AC neighbors), with TT-flanked 3a showing a 3-fold fluorescence enhancement compared to its monomeric form (Fig. 3B). It has the potential to be one of the brightest FBAs in DNA, comparable to previously reported variants such as ABN [28], tsT [29], and 2CNqA [30].

In contrast, the thiophene-modified analog 3b demonstrated superior performance characteristics. The electron-rich thiophene moiety imparted resistance to PET quenching, resulting in more consistent quantum yields (Φem = 0.05–0.08) across all sequence contexts (Fig. 3D and Supplementary Table S10). Notably, 3b exhibited dramatic fluorescence enhancement upon incorporation into DNA,

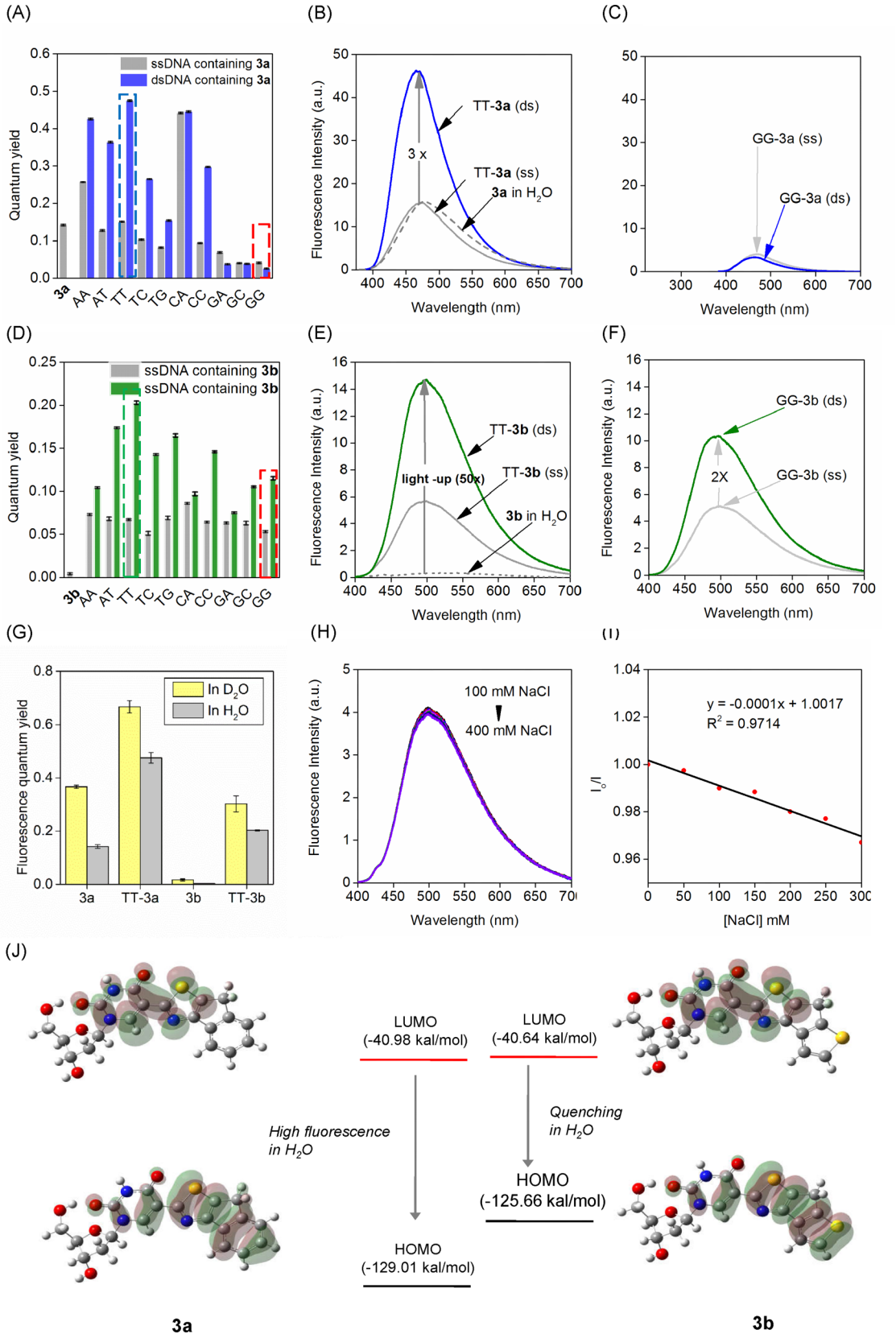

Figure 3. Characterization of 3a- and 3b-incorporated oligonucleotides. (**A**) Fluorescence quantum yields of 3a in ss- or ds-DNA strands in different solvents. (**B**) Fluorescence emission intensity of 3a sandwiched between TT residues and (**C**) GG residues. (**D**) Fluorescence quantum yields of 3b in ss- or ds-DNA strands in different solvents. (**E**) Fluorescence emission intensity of 3b sandwiched between TT residues and (**F**). GG residues. (**G**) Fluorescence emission of 3a and 3b in D_2O and H_2O. (**H–I**) The effect of concentration of Cl^- on the fluorescence emission of 3b in dsDNA. (**J**) Density function theory calculation of the HOMO and LUMO of 3a and 3b.

achieving up to a 10-fold increase in single strands and a remarkable 50-fold increase in duplexes when flanked by TT residues (Fig. 3E and Supplementary Fig. S14). Even in the challenging GG context, 3b maintained significant fluorescence enhancement, with a 5-fold increase in ssDNA and a 10-fold increase in dsDNA compared to its monomeric form (Fig. 3F).

Mechanistic investigation of 3b's fluorescence enhancement in oligonucleotides

To elucidate the unusual fluorescence enhancement of 3b (^{Tz}dU) upon DNA incorporation, we systematically examined four potential mechanisms that typically cause quenching in other FBAs: (i) solvent-induced collisional quenching, (ii) ESPT, (iii) chloride quenching, and (iv) molecular rotor effects. Our findings revealed that 3b's behavior contrasts sharply with conventional fluorescent nucleosides through several key observations.

First, 3b exhibited exceptional sensitivity to water quenching, being 30 times more susceptible than to methanol. This heightened sensitivity elucidates its dramatic fluorescence turn-on in DNA. Water serves as an efficient hydrogen bond donor and polar solvent, facilitating excited-state deactivation through intermolecular electron/proton transfer. The hydrophobic microenvironment of DNA effectively excludes quenching from water molecules, resulting in significant fluorescence activation, specifically, a 10-fold increase in sDNA and up to a 50-fold increase in dsDNA. Further insight was gained from deuterium isotope experiments which demonstrated the critical role of ESPT in aqueous quenching. 3b exhibited substantially brighter emission ($\Phi D_2O/\Phi H_2O = 4.3$) in deuterated water ($D_2O$) compared to regular water (H_2O) (Supplementary Table S11). But when 3b was incorporated in a TT duplex, the quantum yield changed markedly smaller ($\Phi D_2O/\Phi H_2O < 1.5$). This indicates that the duplex structure effectively shielded 3b from ESPT occurring in bulk aqueous solution, which contributed significantly to the fluorescence turn-on of 3b (Fig. 3G) [31]. Third, Stern–Volmer quenching experiments with chloride ions revealed that the fluorescence intensity of 3b is largely unaffected by chloride concentration when incorporated into a matched duplex. This indicates that the duplex structure effectively shields 3b from chloride–induced quenching, thereby excluding chloride–protection as a significant contributor to the fluorescence turn–on behavior of 3b (Fig. 3H and I, and Supplementary Fig. S15) [32]. Finally, the effect of solvent viscosity on the fluorescence of 3b was evaluated in methanol–glycerol mixtures. The results showed that while the fluorescence intensity of 3b is positively correlated with solvent viscosity, the extent of enhancement is very limited. This indicates that 3b exhibits only negligible molecular rotor character [33–35], and that the fluorescence enhancement observed in the duplex cannot be attributed to viscosity–restricted intramolecular rotation. (Supplementary Figs S6 and S7).

To further investigate the electronic basis of these observations, we conducted density functional theory (DFT) calculations. In the ground state, the highest occupied molecular orbital (HOMO) of both 3a and is delocalized across the tricyclic thiazole system, while the lowest unoccupied molecular orbital (LUMO) is localized on the pyrimidine ring, indicating a push-pull character with charge transfer from the benzene (3a) or thiophene (3b) donor to the pyrimidine acceptor upon excitation (Fig. 3J) [22].

DFT calculations also revealed distinct HOMO energy levels relative to guanine (Supplementary Fig. S8 and Supplementary Table S5). The thiophene group in 3b elevates its HOMO energy (-125.55 kcal mol^{-1}) substantially above guanine (-131.24 kcal mol^{-1}), creating a 5.7 kcal mol^{-1} energy gap. In contrast, 3a's HOMO (-129.01 kcal mol^{-1}) lies much closer to guanine's, consistent with the efficient quenching observed when 3a is flanked by guanine residues (Fig. 3C). Although the HOMO energy difference between 3a and 3b is modest, their divergent PET behavior may additionally reflect differences in conformational flexibility and orbital overlap within the DNA duplex.

Collectively, these results indicate that the fluorescence turn-on of 3b involves escape from aqueous quenching pathways, while the HOMO energy calculations rationalize its resistance to guanine-mediated quenching. A more detailed mechanistic discussion is provided in the Discussion section.

Enzymatic incorporation of fluorescent nucleoside triphosphates 6a and 6b

The enzymatic incorporation of nucleoside triphosphates is essential for diagnostic applications such as real-time PCR and genomic DNA labeling. To evaluate this capability, we converted 3a and 3b into their triphosphate forms (6a and 6b) and tested them in standard molecular biology techniques, including PEX and PCR. Their enzymatic incorporation efficiency was assessed using conventional DNA polymerases [39, 40]. PEX assays conducted with Deep Vent DNA polymerase demonstrated the successful incorporation of both nucleoside triphosphates (6a and 6b) into DNA strands (scheme illustrated in Fig. 4A and Supplementary Table S12) [41]. Denaturing polyacrylamide gel electrophoresis (PAGE) analysis confirmed product formation with single or multiple incorporations of 3a and 3b, showing no detectable incomplete byproducts (Fig. 4B and E, and Supplementary Fig. S16). Furthermore, the intrinsic fluorescence properties of the fluorescent nucleosides also allowed for direct monitoring of the incorporation process via fluorescence monitoring. Notably, single incorporation of 3b resulted in a 25-fold enhancement in fluorescence for extended dsDNA products compared to the free triphosphate (Fig. 4D). By contrast, incorporation of 3a residues via PEX, single or multiple, only generated a modest fluorescence enhancement of 2-fold (Fig. 4C and F). Additionally, multiple incorporation experiments using KOD XL polymerase were also conducted and 43-mer products containing up to four 3b modifications were yielded, which exhibited an 18-fold increase in brightness (Fig. 4G). These results confirm the efficient enzymatic incorporation of both fluorescent analogs while preserving their advantageous turn-on fluorescence properties.

In PCR experiments with KOD XL DNA polymerase, complete replacement of dTTP with either 6a or 6b abolished amplification (Supplementary Table S13). However, partial substitution was successful, as confirmed by both PAGE and fluorescence measurements (Supplementary Figs S17–S20). To determine the lowest practical incorporation ratio detectable by fluorescence in the PCR assay, we performed a titration series of 6b against natural dTTP, including 3:1, 2:1, 1:1, 1:2, 1:3, and 1:4. Our results indicate that a 6b : dTTP ratio of 1:2

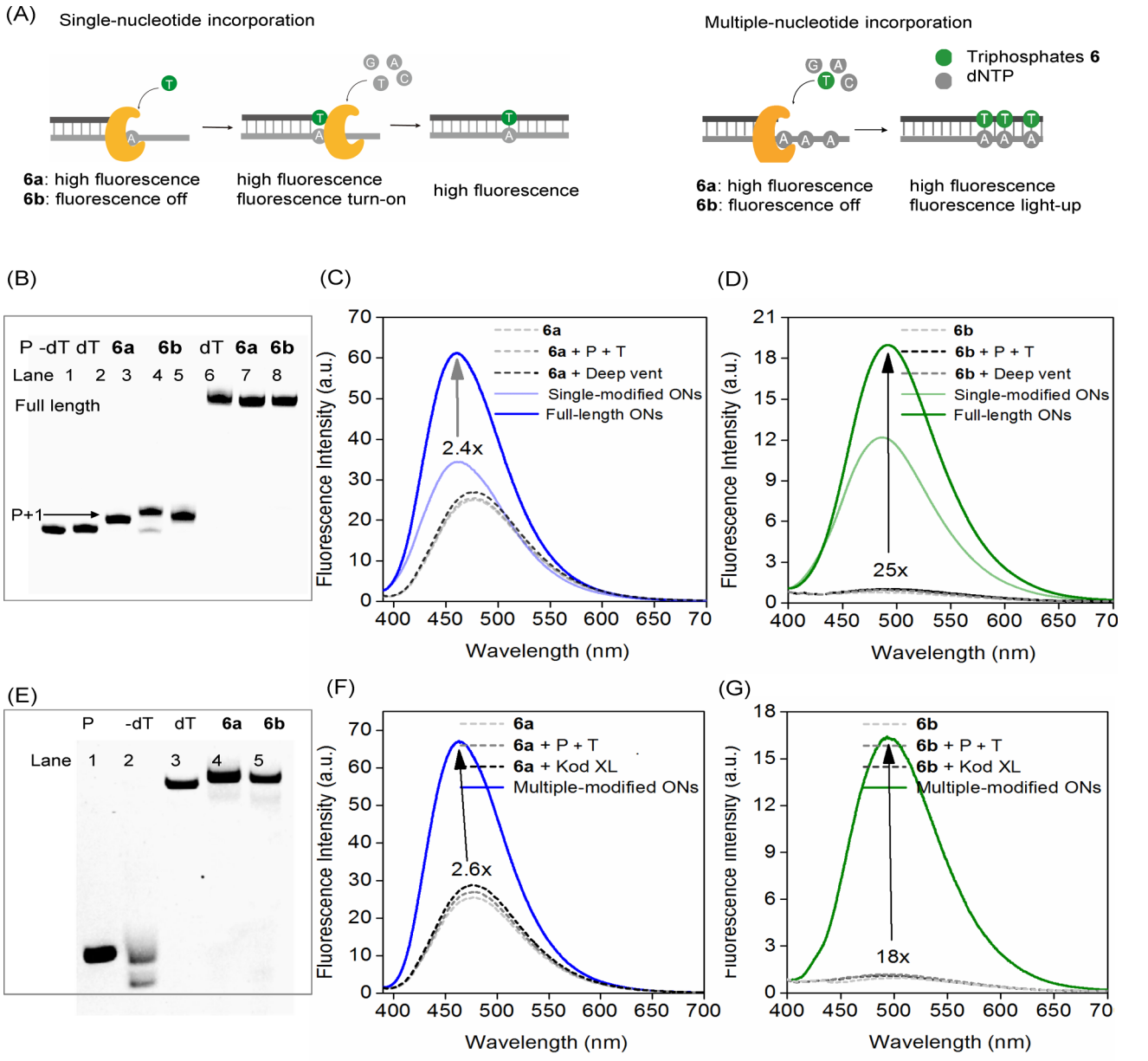

Figure 4. (**A**) Scheme of PEX incorporation of 6a and 6b into dsDNA. (**B**) PAGE analysis of PEX using dTTP or 6a or 6b with Deep vent DNA polymerase for singe incorporation. Lane 1: primer; lane 2: PEX without dTTP; lane 3–8: PEX with dTTP, 6a or 6b with 43-mer (lanes 3–5) or 98-mer (lanes 6–8) template. (**C**) Fluorescence spectra of PEX products with single 6a or. (**D**) 6b. (**E**) PAGE analysis of PEX using dTTP or 6a or 6b using KOD XL DNA polymerase for multiple incorporation. Lane 1: primer, lane 2: PEX without dTTP, lane 3–8: PEX with dTTP, 6a or 6b with 43-mer (lanes 3–5) or 98-mer (lanes 6–8) template. (**F**) Fluorescence spectra of PEX product with multiple 6a or (**G**) 6b.

(33.3% substitution) is the minimum ratio that can be reliably incorporated by the polymerase to generate a PCR amplicon with a fluorescence signal consistently distinguishable from the background noise. For 6b, the polymerase tolerated up to 75% substitution ([6b]:[dTTP] = 3:1) with shorter 98 bp templates, while longer 321 bp templates required a more conservative 60% substitution. Similar substitution thresholds were observed for 6a. Furthermore, the higher endpoint fluorescence intensity for 6a relative to 6b (Fig. 4F and G, and Supplementary Fig. S21) suggests that 6a is incorporated more efficiently by the enzyme under these conditions. Although PCR efficiency was reduced compared to natural dNTPs, the intrinsic fluorescence of these analogs eliminates the need for exogenous detection dyes.

These results demonstrate that both analogs perform efficiently in PEX, with 3b exhibiting superior fluorescence turn-on properties. While PCR necessitates partial dTTP substitution, this system allows for fluorescent PCR with label-free detection. These nucleosides present valuable alternatives for sensitive, self-reporting nucleic acid probes, particularly in applications requiring high signal-to-background ratios.

To preliminarily explore the potential of triphosphate 6b for nuclear labeling in live cells, we used a synthetic nucleotide triphosphate transporter (SNTT) to deliver 6b into U–2 OS cells [39]. Confocal microscopy revealed detectable but weak fluorescence in the nuclear region (Supplementary Fig. S27), with Cy3–dUTP serving as a positive control. The nuclear localization suggests successful delivery and possible DNA la-

beling. Unfortunately, despite our attempts to visualize discrete replication foci, no clear foci were detected, which may stem from the intrinsically low brightness of 3b.

Gradient illumination of DNA by 3b (TzdU) and its application

We conducted a systematic investigation into the fluorescence emission properties of DNA strands containing multiple ^{Tz}dU residues through PEX experiments. To ensure the broad applicability of ^{Tz}dU-incorporated oligonucleotides, we used randomly generated DNA template sequences to avoid biases from manual selection. This approach allowed the adenosine in the template to be flanked by diverse base pairs, including GC, TT, and GT. DNA templates of varied lengths were designed to incorporate 1 to 6 ^{Tz}dU residues, evenly distributed and separated by every 9 bases (Supplementary Tables S14 and S16). To clearly distinguish the template from the product, we employed a FAM-labeled primer and analyzed the PEX products using denaturing PAGE, visualizing the results in the FAM channel (Fig. 5B and C). The results confirmed the efficient incorporation of ^{Tz}dU into the DNA strands. To obtain the fluorescence signals of the PEX products without interference from FAM, we conducted the PEX experiment using primers that were not FAM-labeled. We then measured the fluorescence signals of the PEX products in the ^{Tz}dU emission channel. The results indicated that single incorporation of ^{Tz}dU increased the emission intensity by approximately 5-fold compared to the free nucleoside monomer. Moreover, the intensity enhancement demonstrated a near-proportional correlation to the number of incorporated ^{Tz}dU residues (Fig. 5D and E).

The fluorescence intensity of the overall reaction can be modulated by incorporating varying numbers of ^{Tz}dU residues. We draw a direct analogy between this phenomenon and electronic displays, where the brightness is controlled by the number of electrons. Inspired by this fundamental parallel, we introduced T^{z}dU as a novel modality for information visualization (Fig. 5A). On a 96-well plate, we created both a face pattern and a "2025" numeral display by arranging PEX products containing varying numbers of ^{Tz}dU residues in specific wells. Fluorescence measurements were converted to heatmaps that accurately reproduced the intended patterns (Fig. 5F and G, and Supplementary Figs S22 and S23). This successful demonstration underscores the potential of ^{Tz}dU as a brightness-based visualization material.

Leveraging the unique numerical and fluorescence-related properties of ^{Tz}dU, we further explored its potential application in molecular information encryption as a proof-of-concept study (Fig. 5H). The key advances lie in exploring the quantitative fluorescence response of ^{Tz}dU to encode numerical information, thereby enabling a hybrid encryption strategy that combines fluorescence-based key storage with sequence-based DNA information storage.

In this framework, the original information was first encrypted using the widely adopted Blowfish algorithm [40], which generated a key and the corresponding ciphertext. The key was stored using oligonucleotides containing defined numbers of ^{Tz}dU residues, with each numerical digit mapped to a characteristic fluorescence intensity (Supplementary Table S15). In parallel, the ciphertext was encoded into three DNA strands using the previously established Wukong codec (Supplementary Fig. S24) [41]. These sequences were inserted into plasmids and transformed into *E. coli* for data storage and replication (Fig. 5I). Information retrieval was achieved through fluorescence readout for key reconstruction and DNA sequencing for ciphertext recovery. To validate this approach, a Chinese poem was encrypted as a representative example. The numerical key (13 456) was accurately reconstructed by measuring fluorescence intensities and mapping them to their corresponding numerical digits, while the ciphertext-encoded DNA sequences were successfully read from the plasmid collected from *E.* coli, even after thousands of generations (Fig. 5J–L, and Supplementary Figs S25 and 26). Ciphertext was obtained by decoding with Wukong, and subsequently, decryption was achieved by Blowfish algorithm with the retrieved key and ciphertext. These results demonstrate that the unique numerical and fluorescence properties of ^{Tz}dU can be integrated with established cryptographic and DNA storage tools to enable robust molecular information encryption.

By expanding the molecular alphabet, the base analog could increase the encoding space and potential complexity of encryption, thereby providing additional degree of freedom for information security. In this regard, although the applications for ^{Tz}dU are likely more extensive, these results establish it as a promising candidate for information management.

Discussion

Over the past few decades, significant efforts have been dedicated to developing fluorescent nucleosides for DNA visualization in biotechnological applications. While numerous analogs, such as 2-aminopurine (2AP), have proven valuable for studying nucleic acid-protein interactions, most exhibit fundamental limitations. These include high quantum yields ($\Phi = 0.6$–0.7) in aqueous solutions that decrease upon DNA incorporation due to quenching from neighboring bases, primarily through π–π stacking and collisional mechanisms. Such effects compromise both imaging precision and probe reliability. As a result, the field has pursued turn-on fluorescent nucleosides to overcome these challenges. However, early examples demonstrated only modest emission increases (typically $<$ 5-fold) and remained sensitive to sequence context.

The development of fluorescent nucleoside ^{Tz}dU represents a significant advance in this field. Comprehensive characterization has uncovered three pivotal properties that collectively distinguish ^{Tz}dU from all previously reported analogs: first, its robust turn-on fluorescence, exhibiting approximately 10-fold enhancement in ssDNA and up to 50-fold enhancement in ds-DNA relative to its weakly fluorescent monomeric state; second, its remarkable sequence insensitivity, ensuring consistent emission independent of adjacent base contexts; and third, its high enzymatic compatibility, which facilitates real-time monitoring of DNA synthesis through efficient incorporation by DNA polymerases.

The remarkable properties of 3b arise from its unique electronic structure and its ability to evade distinct quenching pathways. Crucially, the divergent behavior of 3a and 3b does not originate from ground-state acidity—their pKa values are nearly identical (8.49 versus 8.57)—but rather appears to reflect distinct excited-state dynamics. Based on literature precedents [42–44], the thiophene ring in 3b is proposed to reduce aromaticity within the π-system and engage in specific S···H–O hydrogen-bonding interactions with water, potentially facilitating efficient ESPT quenching in aqueous solution. This interpretation is consistent with the 35-fold quench-

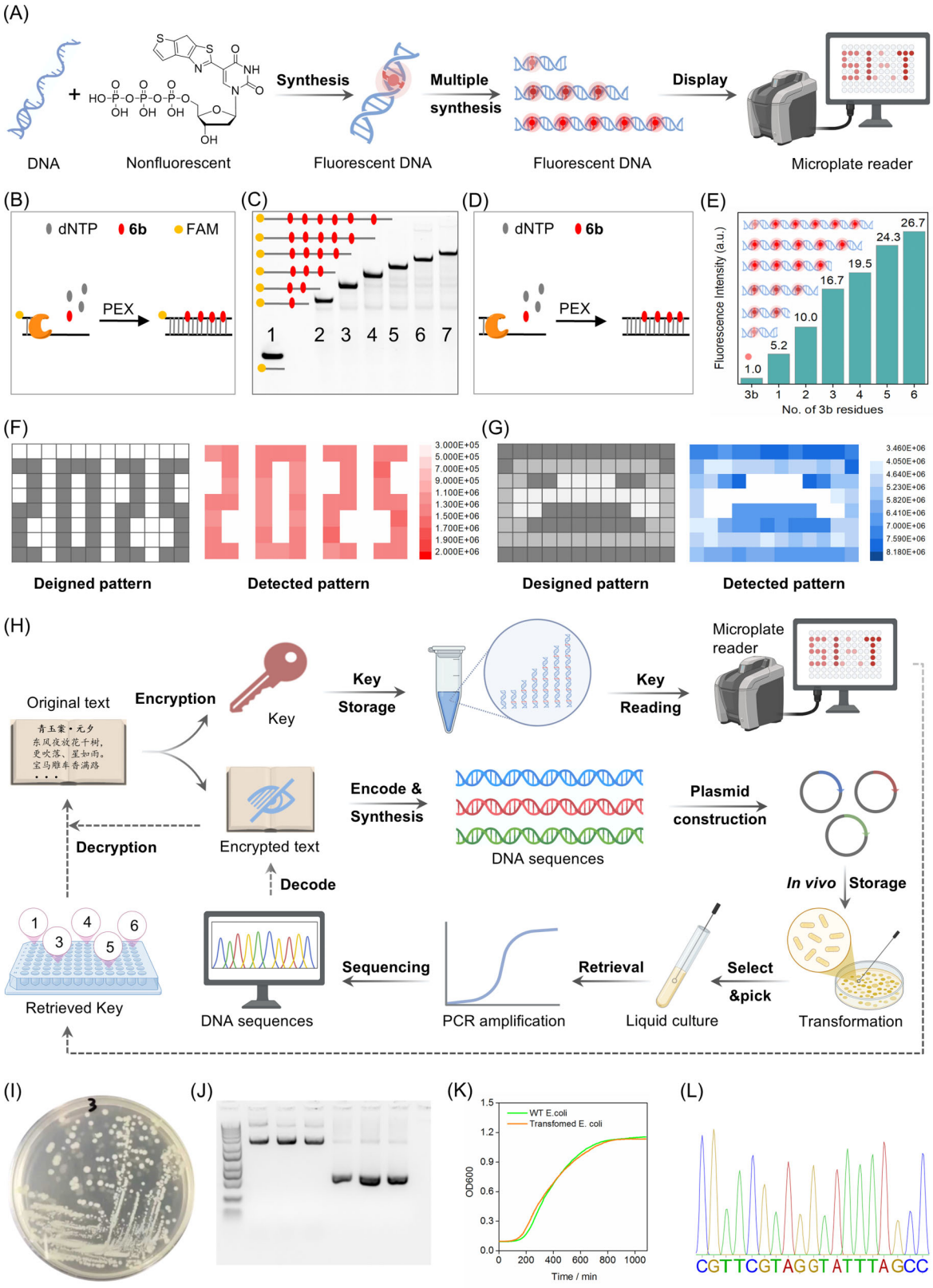

Figure 5. Application of ^{Tz}dU in brightness-based data visualization and encryption. (**A**) Workflow of ^{Tz}dU-incorporated oligonucleotides in data visualization. (**B**) Scheme of PEX incorporation of ^{Tz}dU using Deep vent DNA polymerase with FAM-labeled primer. (**C**) PAGE analysis of the PEX product containing different number of ^{Tz}dU residues, lane 1, primer, lanes 2–7, PEX product containing 1–6 ^{Tz}dU residues, visualized in FAM channel. (**D**) Scheme of PEX incorporation of ^{Tz}dU using Deep vent DNA polymerase with nonfluorescent primer. (**E**) Relative fluorescence intensity of PEX products containing 1–6 ^{Tz}dU residues compared to free ^{Tz}dU. (**F**) Visual effect of ^{Tz}dU-incorporated oligonucleotides displaying patterns of "2025" and (**G**) "face" in 96-well plates. (**H**) Workflow of ^{Tz}dU-incorporated oligonucleotides in numerical key storage and Chinese poem encryption and decryption. (**I**) Single colony selection of constructed plasmids in LB plate. (**J**) Agarose analysis of extracted plasmids and PCR fragments. (**K**) Growth curve of plasmid-transformed and wild-type *E. coli* strains. (**L**) The sequencing results of the extracted DNA encoding the classical Chinese poem.

ing observed for 3b in water relative to methanol. Upon incorporation into DNA which creates a relative hydrophobic environment, where water access is limited, this ESPT pathway is likely suppressed, giving rise to the pronounced 10–50-fold fluorescence turn-on. In contrast, the more aromatic benzene moiety in 3a is expected to interact only weakly with solvent, consistent with its modest water quenching (2.7-fold) and minimal DNA-induced enhancement (∼2-fold).

As an additional observation, DFT calculations suggest a possible rationale for the behavior of 3b in the context of guanine-rich sequences. These calculations suggest that the thiophene moiety elevates the HOMO energy of 3b (−125.55 kcal mol^{-1}) above that of guanine (−131.24 kcal mol^{-1}), creating a 5.7 kcal mol^{-1} energy gap that may disfavor PET. This possible resistance could help 3b retain brightness even when flanked by guanine residues, potentially contributing to its sequence–insensitive emission. The thiophene linker may therefore serve a dual role: it sensitizes 3b toward ESPT in water—establishing a strong quenching baseline that enables high turn-on upon DNA incorporation—while potentially conferring a degree of resistance to guanine-mediated PET, thereby supporting sequence-insensitive emission. This combination of effects offers a plausible rationale for the high turn-on ratio and sequence insensitivity observed for 3b, and suggests a potential design strategy for next-generation fluorescent nucleoside analogs.

The successful incorporation of 3b triphosphate by DNA polymerases in PEX assays and PCR highlights its utility for fluorescent DNA detection in sensing applications. Notably, the fluorescence turn-on effect of 3b is modulated in a template DNA-dependent manner, yielding a graded response. Analogous to an electronic oscilloscope rendering images using varying electron densities, the ability to control fluorescence within DNA sequences offers a possibility of 3b to display images. This tunable fluorescence further suggests potential applications in information encoding, where different intensity levels could represent distinct data states. As a proof-of-concept study, we demonstrated the construction of a dual-layer encryption system in which primary data is encoded within the DNA sequence, while the decryption key is embedded in the fluorescence response generated by 3b, readable via a microplate reader. This approach demonstrates how fluorescence-based readout can complement sequence-based information, adding a supplementary dimension to molecular encryption strategies.

Conclusions

In this study, we developed an efficient synthetic route for novel thymidine analogs, successfully achieving ^{Tz}dU in a 52% yield over seven steps without the need for chromatographic purification. ^{Tz}dU represents a significant breakthrough as the first universal turn-on fluorescent nucleoside, exhibiting negligible fluorescence in water but demonstrating strong, sequence-independent emission enhancement upon DNA incorporation—specifically, a 10-fold increase in ssDNA and up to a 50-fold increase in dsDNA. Unlike conventional FBAs, which are often affected by neighbouring base quenching, ^{Tz}dU exhibited minimal fluctuation in fluorescence intensity across all sequence contexts while preserving the integrity of DNA structure. Its modified triphosphate is efficiently incorporated by Deep Vent and KOD XL polymerases, enabling real-time monitoring of enzymatic reactions.

The unique photophysical properties of ^{Tz}dU, which combine sequence-insensitive brightness with structural compatibility, effectively address long-standing challenges in fluorescent nucleoside design. Mechanistic studies elucidate that ^{Tz}dU escapes aqueous quenching pathways when incorporated into DNA. Although its potential applications are diverse, the template-dependent fluorescence modulation of ^{Tz}dU supports its use in DNA-based data visualization and encryption as an example of practical utility. The unprecedented combination of robust turn-on fluorescence, sequence independence, and enzymatic compatibility opens new doors for advancing both fundamental understanding and practical applications of FBAs, while the feasible synthetic route facilitates widespread adoption.

Acknowledgements

We thank members of the Mei laboratory for helpful suggestions and comments on the manuscript. We are grateful to the Shenzhen Infrastructure for Synthetic Biology and the National Industrial Innovation Center for Bio-manufacturing for instrument support and technical assistance.

Author contributions: Jinsi Li (Data curation [equal], Formal analysis [equal], Investigation [equal], Methodology [equal], Writing – original draft [equal]), Ziwen Dai (Data curation [equal], Investigation [equal], Methodology [equal], Validation [equal], Visualization [equal], Writing – original draft [equal], Writing – review & editing [equal]), Lei He (Formal analysis [supporting], Investigation [equal], Methodology [supporting], Visualization [supporting], Writing – original draft [supporting]), Jiaxin Xu (Formal analysis [supporting], Investigation [supporting], Methodology [supporting], Visualization [supporting], Writing – original draft [supporting]), Chenghe Xiong (Data curation [supporting], Investigation [supporting], Methodology [supporting], Writing – original draft [supporting]), Junlin Wen (Investigation [supporting], Methodology [supporting]), Jingwei Zhou (Software [equal], Visualization [equal], Writing – original draft [supporting]), Xuan Feng (Investigation [supporting], Methodology [supporting]), Xue Chen (Data curation [supporting]), Xia Li (Data curation [supporting]), Lu Zhou (Investigation [supporting], Methodology [supporting], Visualization [supporting]), Chenguang Lou (Data curation [supporting], Supervision [supporting], Writing – review & editing [supporting]), Xiaoluo Huang (Project administration [equal], Resources [equal], Software [equal], Writing – original draft [equal], Writing – review & editing [equal]), Ming Xin (Conceptualization [equal], Data curation [equal], Supervision [equal], Validation [equal], Writing – original draft [equal], Writing – review & editing [equal]), and Hui Mei (Conceptualization [equal], Funding acquisition [lead], Project administration [lead], Supervision [lead], Writing – original draft [equal], Writing – review & editing [lead])

Supplementary data

Supplementary data is available at NAR online.

Conflict of interest

The authors have a pending patent application in China related to the information storage method described in this article.

Funding

This work was supported by the National Key R&D Program of China (Grant No. 2021YFF1201700); Guangdong Provincial Key Laboratory of Synthetic Genomics (2023B1212060054); Shenzhen Key Laboratory of Synthetic Genomics (SYSPG20241211173920047); Shenzhen Institute of Synthetic Biology Scientific Research Program (JCHZ20210002); Shenzhen Science and technology Program (JCYJ20250604142426036). Funding to pay the Open Access publication charges for this article was provided by the Shenzhen Institutes of Advanced Technology.

Data availability

The data underlying this article are available in the article and in its online supplementary material.

References

1. Khatik SY, Srivatsan SG. Environment-sensitive nucleoside probe unravels the complex structural dynamics of i-motif DNAs. *Bioconjug Chem* 2022;33:1515–26. https://doi.org/10.1021/acs.bioconjchem.2c00237
2. Tanpure AA, Srivatsan SG. Conformation-sensitive nucleoside analogues as topology-specific fluorescence turn-on probes for DNA and RNA G-quadruplexes. *Nucleic Acids Res* 2015;43:e149. https://doi.org/10.1093/nar/gkv743
3. Sholokh M, Sharma R, Grytsyk N *et al.* Environmentally sensitive fluorescent nucleoside analogues for surveying dynamic interconversions of nucleic acid structures. *Chem A Eur J* 2018;24:13850–61. https://doi.org/10.1002/chem.201802297
4. Dziuba D, Didier P, Ciaco S *et al.* Fundamental photophysics of isomorphic and expanded fluorescent nucleoside analogues. *Chem Soc Rev* 2021;50:7062–107. https://doi.org/10.1039/D1CS00194A
5. Sinkeldam RW, Greco NJ, Tor Y. Fluorescent analogs of biomolecular building blocks: design, properties, and applications. *Chem Rev* 2010;110:2579–619.
6. Yang S, Bögels BWA, Wang F *et al.* DNA as a universal chemical substrate for computing and data storage. *Nat Rev Chem* 2024;8:179–94. https://doi.org/10.1038/s41570-024-00576-4
7. Li J, Crown A, Ney P *et al.* Hybridization-encoded DNA tags with paper-based readout for anti-forgery raw material tracking. *Nat Commun* 2025;16:5832.
8. Jean JM, Hall KB. 2-Aminopurine fluorescence quenching and lifetimes: role of base stacking. *Proc Natl Acad Sci USA* 2001;98:37–41.
9. Thompson KC, Miyake N. Properties of a new fluorescent cytosine analogue, pyrrolocytosine. *J Phys Chem B* 2005;109:6012–9. https://doi.org/10.1021/jp046177n
10. Xu W, Chan KM, Kool ET. Fluorescent nucleobases as tools for studying RNA and DNA. *Nature Chem* 2017;9:1043–55. https://doi.org/10.1038/nchem.2859
11. Sandin P, Börjesson K, Li H *et al.* Characterization and use of an unprecedentedly bright and structurally non-perturbing fluorescent DNA base analogue. *Nucleic Acids Res* 2008;36:157–67. https://doi.org/10.1093/nar/gkm1006
12. Teppang KL, Lee RW, Burns DD *et al.* Electronic modifications of fluorescent cytidine analogues control photophysics and fluorescent responses to base stacking and pairing. *Chem A Eur J* 2019;25:1249–59. https://doi.org/10.1002/chem.201803653
13. Hirashima S, Han JH, Tsuno H *et al.* New size-expanded fluorescent thymine analogue: synthesis, characterization, and application. *Chem A Eur J* 2019;25:9913–9. https://doi.org/10.1002/chem.201900843
14. Ducharme GT, LaCasse Z, Sheth T *et al.* Design of turn-on near-infrared fluorescent probes for highly sensitive and selective monitoring of biopolymers. *Angew Chem Int Ed* 2020;59:8440–4. https://doi.org/10.1002/anie.202000108
15. Burns DD, Teppang KL, Lee RW *et al.* Fluorescence turn-on sensing of DNA duplex formation by a tricyclic cytidine analogue. *J Am Chem Soc* 2017;139:1372–5. https://doi.org/10.1021/jacs.6b10410
16. Kuba M, Kraus T, Rohl R *et al.* Nucleotide-bearing benzylidene-tetrahydroxanthylium near-IR fluorophore for sensing DNA replication and secondary structures. *Chem A Eur J* 2020;26:11950–4. https://doi.org/10.1002/chem.202003192
17. Turner MB, Cizmic JM, Rosansky DB *et al.* Sequence-specific fluorescence turn-on sensing of RNA by DNA probes incorporating the tricyclic cytidine analogue DEAtC. *Bioconjug Chem* 2023;34:1061–71. https://doi.org/10.1021/acs.bioconjchem.3c00134
18. Manna S, Srivatsan SG. Synthesis and enzymatic incorporation of a responsive ribonucleoside probe that enables quantitative detection of metallo-base pairs. *Org Lett* 2019;21:4646–50.10.1021/acs.orglett.9b01544
19. Mata G, Schmidt OP, Luedtke NW. A fluorescent surrogate of thymidine in duplex DNA. *Chem Commun* 2016;52:4718–21. https://doi.org/10.1039/C5CC09552B
20. Li J, Fang X, Ming X. Visibly emitting thiazolyl-uridine analogues as promising fluorescent probes. *J Org Chem* 2020;85:4602–10. https://doi.org/10.1021/acs.joc.9b03208
21. Matsuda A, Itoh H, Takenuki K *et al.* Alkyl addition reaction of pyrimidine 2'-ketonucleosides: synthesis of 2'-branched-chain sugar pyrimidine nucleosides. *Chem Pharm Bull* 1988;36:945–53. https://doi.org/10.1248/cpb.36.945
22. Reichardt C. Solvatochromic dyes as solvent polarity indicators. *Chem Rev* 1994;94:2319–58. https://doi.org/10.1021/cr00032a005
23. Bag SS, Gogoi H. Design of "click" fluorescent labeled 2′-deoxyuridines via C5-[4-(2-propynyl(methyl)amino)]phenyl acetylene as a universal linker: synthesis, photophysical properties, and interaction with BSA. *J Org Chem* 2018;83:7606–21. https://doi.org/10.1021/acs.joc.7b03097
24. Hanaoka K, Iwaki S, Yagi K *et al.* General design strategy to precisely control the emission of fluorophores via a twisted intramolecular charge transfer (TICT) process. *J Am Chem Soc* 2022;144:19778–90. https://doi.org/10.1021/jacs.2c06397
25. Pawar MG, Srivatsan SG. Photophysical characterization and enzymatic incorporation of a microenvironment-sensitive fluorescent uridine analog. *Org Lett* 2011;13:1114–7. https://doi.org/10.1021/ol103147t
26. Greco NJ, Tor Y. Simple fluorescent pyrimidine analogues detect the presence of DNA abasic sites. *J Am Chem Soc* 2005;127:10784–5. https://doi.org/10.1021/ja052000a
27. Samaan GN, Wyllie MK, Cizmic JM *et al.* Single-molecule fluorescence detection of a tricyclic nucleoside analogue. *Chem Sci* 2021;12:2623–8. https://doi.org/10.1039/D0SC03903A
28. Karimi A, Börner R, Mata G *et al.* A highly fluorescent nucleobase molecular rotor. *J Am Chem Soc* 2020;142:14422–6. https://doi.org/10.1021/jacs.0c05180
29. Nogal Wd, A. F, F A *et al.* Getting DNA and RNA out of the dark with 2CNqA: a bright adenine analogue and interbase FRET donor. *Nucleic Acids Res* 2020;48:7640–52.
30. Olmsted J, Kearns DR. Mechanism of ethidium bromide fluorescence enhancement on binding to nucleic acids. *Biochemistry* 1977;16:3647–54. https://doi.org/10.1021/bi00635a022
31. Joung JF, Kim S, Park S. Effect of NaCl salts on the activation energy of excited-state proton transfer reaction of coumarin 183. *J Phys Chem B* 2015;119:15509–15. https://doi.org/10.1021/acs.jpcb.5b09905
32. Sinkeldam RW, Marcus P, Uchenik D *et al.* Multisensing emissive pyrimidine. *ChemPhysChem* 2011;12:2260–5. https://doi.org/10.1002/cphc.201100315

33. Sinkeldam RW, Wheat AJ, Boyaci H *et al.* Emissive nucleosides as molecular rotors. *ChemPhysChem* 2011;12:567–70. https://doi.org/10.1002/cphc.201001002
34. Manna S, Sarkar D, Srivatsan SG. A dual-app nucleoside probe provides structural insights into the human telomeric overhang in live cells. *J Am Chem Soc* 2018;140:12622–33. https://doi.org/10.1021/jacs.8b08436
35. Dziuba D, Pospíšil P, Matyašovský J *et al.* Solvatochromic fluorene-linked nucleoside and DNA as color-changing fluorescent probes for sensing interactions. *Chem Sci* 2016;7:5775–85. https://doi.org/10.1039/C6SC02548J
36. Li Y, Fin A, McCoy L *et al.* Polymerase-mediated site-specific incorporation of a synthetic fluorescent isomorphic G surrogate into RNA. *Angew Chem Int Ed* 2017;56:1303–7. https://doi.org/10.1002/anie.201609327
37. Riedl J, Ménová P, Pohl R *et al.* GFP-like fluorophores as DNA labels for studying DNA–protein interactions. *J Org Chem* 2012;77:8287–93. https://doi.org/10.1021/jo301684b
38. Church GM, Gao Y, Kosuri S. Next-generation digital information storage in DNA. *Science* 2012;337:1628. https://doi.org/10.1126/science.1226355
39. Zawada Z, Tatar A, Mocilac P *et al.*, Transport of nucleoside triphosphates into cells by artificial molecular transporters. *Angew Chem Int Ed* 2018;57:9891–5. https://doi.org/10.1002/anie.201801306
40. Xu J, Wang Y, Chen X *et al.* Multi-layer encryption of medical data in DNA for highly-secure storage. *Materials Today Bio* 2024;28:101221. https://doi.org/10.1016/j.mtbio.2024.101221
41. Huang X, Cui J, Qiang W *et al.* Storage-D: a user-friendly platform that enables practical and personalized DNA data storage. *iMeta* 2024;3:e168. https://doi.org/10.1002/imt2.168
42. Wang X, Yin Y, Liu X *et al.* The regulation of π-linker aromaticity of thiophene derivatives on cyclization and ESPT reaction. *J Photochem Photobiol, A* 2025;469:116584. https://doi.org/10.1016/j.jphotochem.2025.116584
43. Zhou X, Wang X, Cui X *et al.* Theoretical insights into the effect of different numbers of thiophene groups on hydrogen bond interaction and excited-state intramolecular proton-transfer process for flavonoid derivatives. *J Phys Chem A* 2024;128:4020–9. https://doi.org/10.1021/acs.jpca.4c02029
44. Babejová M, Třísková I, Trnková L *et al.* Synthesis, optical, electrochemical, and computational study of benzene/thiophene based D–π–A chromophores *RSC Adv* 2024;14:35424–37. https://doi.org/10.1039/D4RA02668C

Received: October 14, 2025. **Revised:** June 3, 2026. **Accepted:** June 5, 2026